Electronic Research Archive

ERA, 31(5): 2651–2666.
DOI: 10.3934/era.2023134
Received: 18 October 2022
Revised: 16 December 2022
Accepted: 27 February 2023
Published: 09 March 2023

http://www.aimspress.com/journal/ERA

Research article

Inhibition of absence seizures in a reduced corticothalamic circuit via closed-loop control

Yan Xie, Rui Zhu, Xiaolong Tan and Yuan Chai*

School of Mathematics and Physics, Shanghai University of Electric Power, Shanghai 201306, China

* **Correspondence:** Email: chaiyuan@shiep.edu.cn.

Abstract: Inhibition of spike-wave discharges (SWD) was thought to be associated with remission of seizure symptoms in absence epilepsy. In the previous studies, pulse stimulation was applied directly to the brain as an effective means to inhibit SWD. However, this method not only failed to provide a real-time tracking control of the disease, but also caused incalculable damage to the patient's brain tissue. To fill the gap, this work studied the mitigation and elimination effects of SWD by applying single-pulse coordinated resetting stimulation (SCRS) to three different neurons, firstly. Secondly, based on the 2I:2O cortical-thalamic model (2I:2O SCT model), four kinds of m:n on-off SCRS with the same period were compared, and the control efficiency and impulse energy consumption were combined to investigate these different stimulations. Finally, we further optimized the regulation strategies, including the weighted structure of stimulation and closed-loop control. Simulation results show that the weighted stimulation and closed-loop control strategy proposed here further improve control performance by reducing energy consumption, which may be more reliable in applications. Moreover, this study provides a new method for optimizing SCRS by the weighted processing and closed-loop control of electrical pulses to alleviate the absence epileptic state.

Keywords: spike-wave discharges; weighted stimulation; single-pulse coordinated reset stimulation; closed-loop control

1. Introduction

As one of the most common chronic neurological diseases in the world [1], epilepsy affects the daily life of tens of millions of people. In severe cases, it can even be life-threatening, which causes

the premature death rate of epilepsy patients to be one to two times higher than that of the normal population [2,3]. Absence seizure as a branch of many epileptic seizure types [4], generally occurs in childhood. Childhood absence seizure (CAE) syndrome is actually a benign syndrome that remits in most CAE patients in early adolescence [5,6]. At the onset of the absence epilepsy, bilateral symmetric SWD at 3 Hz [7] can be observed in the electroencephalogram (EEG) of the patient [8], which provides a basis for our research.

As early as 1873, Jackson in the UK first proposed that epileptic seizures may originate from the cerebral cortex [9,10]. Since then, people have begun to explore the cerebral cortex accordingly. Penfield and Jasper proposed the concept of central brain epilepsy in the 1950s, which aroused the attention of neuropathic researchers to the cortical-thalamic circuit [11,12]. Such inferences and concepts laid the foundation for subsequent research on neurological diseases. The mean-field model [13] with cortex and thalamus as main structures was proposed by Taylor et al. [14] in 2014 to simulate and research Parkinson's disease. The cortical-thalamic (CT) model proposed by Taylor is made up of four neurons, among which the cortical network structure consists of excitatory pyramidal neurons (EPN) and inhibitory interneurons (IIN), and the thalamic structure is composed of thalamic reticular nucleus (TRN) and specific relay nuclei (SRN). In the same year, Chen et al. [15] found that adding the structure of basal ganglia on the basis of Taylor's CT model has certain research significance in absence epilepsy, so we have the basal ganglia-corticothalamic (BGCT) model. However, simplified studies of the BGCT model have not been carried out, and we do not know which stimulation mode is more suitable for the simplified model.

In the 1980s, neurosurgeons began to implant stimulation electrodes to treat movement disorders [16,17]. Benabid implanted thalamic stimulation systems in patients' brains [18] to control the trembling phenomenon in 1987. Electrical pulse stimulation [19] is an effective treatment for patients with partial seizure or partial secondary generalized seizure, especially for patients with refractory epilepsy [20,21] whose epileptogenic focus are located in important functional areas or cannot be located. Despite the risks, the side effects are far smaller than excision of epileptogenic zone [22,23]. On account of the electrical nerve stimulator needs to be implanted through minimally invasive surgery [24,25] to come into play, it is necessary to reduce energy consumption [26,27] so as to achieve prolong stimulator's life in the programming design process. In 2020, Fan et al. applied the closed-loop control principle in the programming process of electrical nerve stimulator to further advance the process of epilepsy control [28–30]. However, the consumption of stimulus is still a problem, and most pulse stimulation has not realized the real-time control function at present.

The first goal of this study is to reduce computational cost and improve neuromodulation efficiency, and the basal ganglia part of Chen's BGCT model is simplified in this paper. Taking the basal ganglia as a whole, the average discharge rate of substantia nigra pars reticulata (SNr/GPi) was calculated as the fixed input parameter for the simplified model, and the simplified model of 2I:2O was finally obtained. The second goal of this study is to optimize the SCRS by combining energy consumption and therapeutic effect. Firstly, we proposed a constant period m:n on-off SCRS, whose sum of two parameters m and n is guaranteed to be a fixed value. The efficiency and energy consumption of stimulation under different combinations of m and n were compared. Secondly, in order to reduce the energy consumption of electrical stimulator, the concept of the weighted stimulation was proposed, which is to multiply the amplitude and pulse width of original stimulation by the corresponding weight. Finally, the closed-loop control theory was applied to the control of stimulation. The continuous recognition of the mean firing rate of excitatory pyramidal neurons as a

feedback signal realized the real-time control function. The main contribution of this work is to create a simplified model and open up new ways to treat epilepsy. The results show that the presentation of the weighted stimulation can not only improve the energy consumption under the premise of ensuring that the stimulation efficacy is not reduced, but also greatly extend the working life of the electrical stimulator and reduce the secondary injury to patients. It is worth noting that the closed-loop treatment of several kinds of stimulation also enables the modulation scheme to achieve a superior effect.

2. Model and plans

Based on Taylor's CT model in 2014, Chen's BGCT model appended the network structure of the basal ganglia [15]. The basal ganglia network structure contains five neurons, $\Lambda_{BG} \in \{d_1, d_2, p_1, p_2, \zeta\}$, as shown in purple in Figure 1(a). They represented striatal D_1 neurons, striatal D_2 neurons, substantia nigra pars reticulata (SNr), globus pallidus external (GPe) and subthalamic nucleus (STN), respectively. The pink and yellow structures in Figure 1(a). represent cortical and thalamic structures in the Taylor's CT model. The cortex contains $\Lambda_C \in \{e, i\}$, indicating that e = EPN, I = IIN, and the thalamus structure consists of $\Lambda_T \in \{r, s\}$, representing r = TRN, s = SRN. The blue solid/dashed arrows denote inhibitory projections mediated by $GABA_A/GABA_B$, and the red arrows mean excitatory synapses mediated by glutamate.

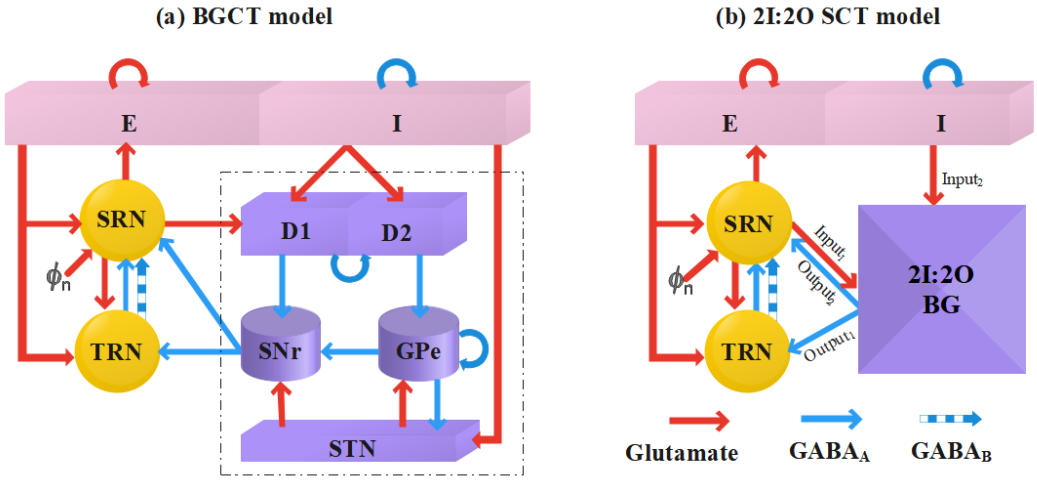

Figure 1. Presentation of models before and after simplification. (a) The referenced BGCT model is composed of a tricolor structure. The pink cortical structures contain excitatory pyramidal neurons (E) and inhibitory interneurons (I), the thalamus in yellow is divided into specific relay nuclei (SRN) and thalamic reticular nucleus (TRN), purple basal ganglia are constructed from striatal D_1 neurons, striatal D_2 neurons, substantia nigra pars reticulata (SNr), globus pallidus external (GPe) and subthalamic nucleus (STN), red and blue arrows represent excitatory or inhibitory projections. (b) In the simplified 2I:2O SCT model, the structure of the cortex and thalamus is unchanged, and all purple structures are divided into a group, and there are only two inhibitory output signals for the cortex and thalamus when modeling.

To calculate the mean firing rate R_a, we needed to know the values of the following parameters: maximum firing rate R_a^{max}, the threshold θ_a of the mean firing rate, and change rate σ of θ_a. Employing the method of mean field model, the mean membrane potential V_a of each neuron can be expressed by an S-shaped function of R_a [31,32].

$$R_a(\mathbf{r},t) = \Gamma[V_a(\mathbf{r},t)] = \frac{R_a^{max}}{1+\exp[-\frac{\pi(V_a(\mathbf{r},t)-\theta_a)}{\sqrt{3}\sigma}]}, \tag{1}$$

where $a \in \Lambda = \{\Lambda_{BG}, \Lambda_C, \Lambda_T\}$ and Λ including all neurons in Figure 1(a). Until V_a exceeds θ_a, the neural population strikes the action potential at mean firing rate R_a, and the S-shaped function keep R_a below R_a^{max} and meet the biological rationality. The variation of the mean membrane potential V_a at position $\mathbf{r}$ is caused by the filtered postsynaptic potential of other nerve populations in the dendrites, modeled as [33, 34]:

$$D_{\alpha\beta}V_a(\mathbf{r},t) = \sum_{b\in\Lambda} C_{ab}\cdot\phi_b(\mathbf{r},t), \tag{2}$$

$$D_{\alpha\beta} = \frac{1}{\alpha\beta}\left[\frac{\partial^2}{\partial t^2} + (\alpha+\beta)\frac{\partial}{\partial t} + \alpha\beta\right], \tag{3}$$

where α and β are the decay and rise time of cell body response to input signal respectively, and $D_{\alpha\beta}$ is the differential operator meaning the dendritic filtering of input signal. C_{ab} describes the coupling strength between neural population b and neural population a. ϕ_b is the rate of afferent pulses received by other neurons from neuron b. In particular, for $GABA_B$-mediated inhibitory projection, a delay τ is introduced in the afferent pulse rate of TRN ϕ_r to simulate its slow synaptic dynamics. $V_i = V_e$ and $R_i = R_e$ are defined, because the intercortical connections are proportional to the number of synapses involved.

Except for excitatory pyramidal neurons, the afferent pulse rate ϕ_c of remaining neurons $c \in \{\Lambda_{BG}, i, \Lambda_T\}$ can be directly depicted by the mean firing rate R_c due to their too-short axon characteristics. However, neuron e has a sufficiently long axon structure, its propagation process can be approximated by a damped wave equation [35]:

$$\frac{1}{\gamma_e^{\,2}}[\frac{\partial^2}{\partial t^2} + 2\gamma_e\frac{\partial}{\partial t} + \gamma_e^{\,2} - C_e^{\,2}\nabla^2]\phi_e(\mathbf{r},t) = R_e(\mathbf{r},t). \tag{4}$$

In Eq (4), γ_e is the time damping rate of the pulse, and ∇^2 is the Laplace operator. The generalized spike-wave discharges during absence seizures are synchronous across the brain, so we assumed that the activity space in the system is uniform, which means $\nabla^2 = 0$. Therefore, the axon field ϕ_e of neuron e can be further written as [36]:

$$\frac{1}{\gamma_e^{\,2}}[\frac{d^2}{dt^2} + 2\gamma_e\frac{d}{dt} + \gamma_e^{\,2}]\phi_e(t) = R_e(t), \tag{5}$$

The dynamic properties of all neural groups were simulated by first-order formal differential

equations. The initial BGCT model could be expressed as follows [17,37]:

$$\frac{\mathrm{d}\phi_e(t)}{\mathrm{d}t} = \dot{\phi}_e(t), \tag{6}$$

$$\frac{\mathrm{d}\dot{\phi}_e(t)}{\mathrm{d}t} = \gamma_e^2[-\phi_e(t) + \Gamma(V_e(t))] - 2\gamma_e\dot{\phi}_e(t), \tag{7}$$

when,

$$X_1(t) = \left[V_e(t), V_{d_1}(t), V_{d_2}(t), V_{p_1}(t), V_{p_2}(t), V_\zeta(t), V_r(t), V_s(t)\right]^{\mathbf{T}}, \tag{8}$$

$$\frac{\mathrm{d}X_1(t)}{\mathrm{d}t} = \dot{X}_1(t), \tag{9}$$

$$\frac{\mathrm{d}\dot{X}_1(t)}{\mathrm{d}t} = \alpha\beta M_1(t) - (\alpha+\beta)\dot{X}_1(t), \tag{10}$$

$$M_1(t) = C_1\Gamma_1(t) - V_1(t), \tag{11}$$

with,

$$C_1 = \begin{bmatrix} C_{ee} & C_{ei} & 0 & 0 & 0 & 0 & 0 & (0,0) & C_{es} \\ C_{d_1e} & 0 & C_{d_1d_1} & 0 & 0 & 0 & 0 & (0,0) & C_{d_1s} \\ C_{d_2e} & 0 & 0 & C_{d_2d_2} & 0 & 0 & 0 & (0,0) & C_{d_2s} \\ 0 & 0 & C_{p_1d_1} & 0 & 0 & C_{p_1p_2} & C_{p_1\zeta} & (0,0) & 0 \\ 0 & 0 & 0 & C_{p_2d_2} & 0 & C_{p_2p_2} & C_{p_2\zeta} & (0,0) & 0 \\ C_{\zeta e} & 0 & 0 & 0 & 0 & C_{\zeta p_2} & 0 & (0,0) & 0 \\ C_{re} & 0 & 0 & 0 & C_{rp_1} & 0 & 0 & (0,0) & C_{rs} \\ C_{se} & 0 & 0 & 0 & C_{sp_1} & 0 & 0 & (C_{sr}^A, C_{sr}^B) & 0 \end{bmatrix}, \tag{12}$$

$$\Gamma_1 = \left[\phi_e, \Gamma(V_e), \Gamma(V_{d_1}), \Gamma(V_{d_2}), \Gamma(V_{p_1}), \Gamma(V_{p_2}), \Gamma(V_\zeta), \left(\Gamma(V_r), \Gamma(V_r(t-\tau))\right), \Gamma(V_s)\right]^{\mathbf{T}}, \tag{13}$$

$$V_1 = \left[V_e(t), V_{d_1}(t), V_{d_2}(t), V_{p_1}(t), V_{p_2}(t), V_\zeta(t), V_r(t), V_s(t) - \phi_n\right]^{\mathbf{T}}, \tag{14}$$

In order to simplify the model, the basal ganglia was regarded as a collective in this paper, so the cortex and thalamus would receive two inhibitory inputs from the basal ganglia and output two excitatory signals. The simplified model was called 2I:2O SCT model, and SCRS were added into neurons *e*, *s* and *r*, respectively. For the simplified model, the expression of the axon field ϕ_e of neuron *e* still adopted Eqs (6) and (7), and the dynamic characteristics of other neurons could be calculated according to the following equation:
when,

$$X_2(t) = \left[V_e(t), V_r(t), V_s(t)\right]^{\mathbf{T}}, \tag{15}$$

$$\frac{\mathrm{d}X_2(t)}{\mathrm{d}t} = \dot{X}_2(t), \tag{16}$$

$$\frac{\mathrm{d}\dot{X}_2(t)}{\mathrm{d}t} = \alpha\beta M_2(t) - (\alpha+\beta)\dot{X}_2(t), \tag{17}$$

$$M_2(t) = C_2\Gamma_2(t) - V_2(t) + S(t), \tag{18}$$

with,

$$C_2 = \begin{bmatrix} C_{ee} & C_{ei} & 0 & (0,0) & C_{es} \\ C_{re} & 0 & C_{rp_1} & (0,0) & C_{rs} \\ C_{se} & 0 & C_{sp_1} & \left(C_{sr}^A, C_{sr}^B\right) & 0 \end{bmatrix}, \tag{19}$$

$$\Gamma_2 = \left[\phi_e, \Gamma\left(V_e\right), \overline{\Gamma\left(V_{p_1}\right)}, \left(\Gamma\left(V_r\right), \Gamma\left(V_r\left(t-\tau\right)\right)\right), \Gamma\left(V_s\right)\right]^{\mathbf{T}}, \tag{20}$$

$$V_2 = \left[V_e(t), V_r(t), V_s(t) - \phi_n\right]^{\mathbf{T}}, \tag{21}$$

$$S = \left[S_e(t), S_r(t), S_s(t)\right]^{\mathbf{T}}, \tag{22}$$

here, $S_e(t)$, $S_r(t)$, $S_s(t)$ represent single-pulse coordinated resetting signals SCRS applied to neurons *e*, *r* and *s*, respectively in Eq (22). Pulse signals were obtained from the following formula [38,39]:

$$\begin{aligned} S(t) &= A_0 \times H\left(\sin\left(\frac{2\pi t}{f_0}\right)\right)\left(1 - H\left(\sin\left(\frac{2\pi(t+\delta)}{f_0}\right)\right)\right), \\ S_x(t) &= \sum_{x=1}^{3} \rho_x(t) S(t). \end{aligned} \tag{23}$$

In the stimulus expression, A_0 represents the amplitude of the pulse, δ_0 denotes the pulse width of the stimulus signals, T_0 determines the cycle of the stimulus, from which we can calculate the frequency of the stimulus as $T_0 = 1/f_0$. *x* equal 1, 2, or 3 correspond to electrode inputs in neurons *e*, *s*, *r*, respectively.

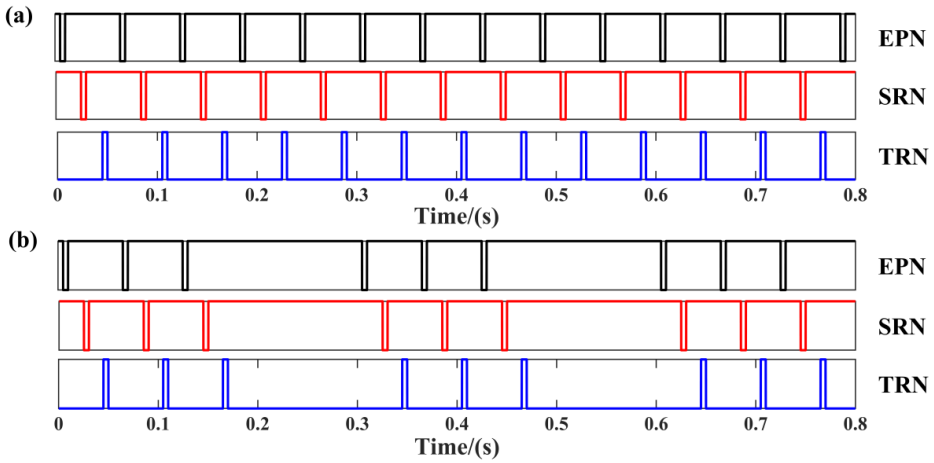

Figure 2. Coordinated release of periodic impulses on three neurons. (a) on-on SCRS (b) 3:2 on-off SCRS. In this paper, the following values are used for stimulus parameters: A_0 = 200 mA, f_0 = 50 Hz, δ_0 = 3.5 ms.

The process of stimulation was equivalent to a process of epilepsy treatment. Electrical stimulators needed to be implanted into patients' cerebral cortex in a minimally invasive way, so the research needed to reduce the energy consumption of electrical pulses as much as possible to ensure the life of electrical stimulators. The calculation method of energy consumption was as follows [40]:

$$Q_{SARS} = \frac{1}{\sqrt{N}} \| S_x(t) \|_2, \tag{24}$$

where N is the total time step, and $\| S_x(t) \|$is the two-norm of $S_x(t)$. To quantify the reduction rate of SWD, the parameter plane ($-C_{sr}$, C_{es}) is divided into 21×21 grid points. In particular, the stimulus efficacy (E) is quantitatively calculated by the grid points Before (B) and After (A) stimulus [41]:

$$E = \left(1 - \frac{A}{B}\right) \times 100\%. \tag{25}$$

In the MATLAB R2018b environment, the fourth-order Runge-Kutta method was used to solve the differential equations, and the total duration of simulation was set as 15 seconds to complete the simulation process. In order to ensure the accuracy and stability of the simulation, we set up the temporal resolution to 0.00005s, and conducted dynamic analysis of neurons from the 5ths. If there were no special instructions in the text, the data referred to previous studies [31,40–42].

3. Results and discussion

3.1. Model analysis before and after simplification

Considering the objective of SCRS, we selected the coupling coefficients $-C_{sr}$ and C_{es} of the

two pathways related to these three neurons. Initially, we plotted the dynamic state frequency diagram of BGCT and 2I:2O SCT model, as shown in Figures 3(a)–(d). There were several relationships between the excitatory cortical firing rate and time under certain coupling strength. According to the characteristics of the excitatory cortical discharge diagram shown in Figure 3(f), states can be divided into two categories, non-oscillation and oscillation. The non-oscillation waveform had no obvious movement trend after stabilization, and was mainly divided into low firing (IV) and high saturation (I). The way to distinguish these two states was to observe the position of discharge rate after stabilization (i.e., 5s). The waveform characteristic of oscillations was periodic. By combining the states (III) and (II) in bifurcation diagram Figure 3(e), it can be determined that one or two sets of peaks and troughs within a unit period was a straightforward way to distinguish simple oscillation (III) from SWD (II).

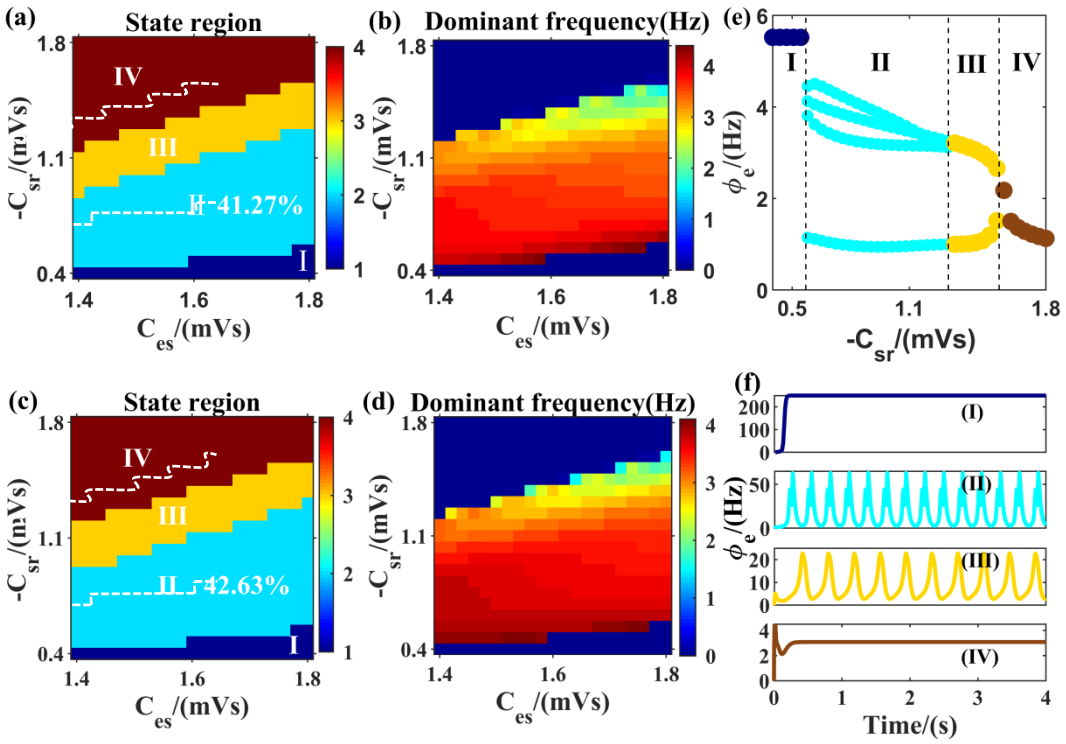

Figure 3. Dynamic analysis of original model and simplified model. (a)-(b), state and frequency diagrams for ϕ_e as a function of BGCT model; (c)-(d), state and frequency diagrams of 2I:2O SCT model, and the boundary position of epileptic state is marked by white lines in the state diagram (c), white lines are used to divide the boundary position of epileptic state. The bifurcation diagram (e) shows the number of peaks and troughs in waveform charts under different coupling strength $-C_{sr}$ with C_{es} = 1.8mVs, corresponding to the four states in discharge charts (f) respectively. When $-C_{sr}$ = 0.4mVs, the state is high saturation (I); when $-C_{sr}$ = 0.8mVs, the state is SWD (II); when $-C_{sr}$ = 1.4mVs, the state is simple oscillation (III); when $-C_{sr}$ = 1.8mVs, the state is low firing (IV).

It can be seen that the white line in Figure 3(c) refers to the boundary position of epileptic state. In Figure 4, we plot the triggering mean discharge rate (TMFR) of different neurons under Figure 3(c) critical position. Furthermore, we completed the fitting of the high/low TMFR so as to obtain the

orange/purple line. The simplified model accelerated the running speed of the mean field model and facilitated the stimulation prioritization in the following two chapters.

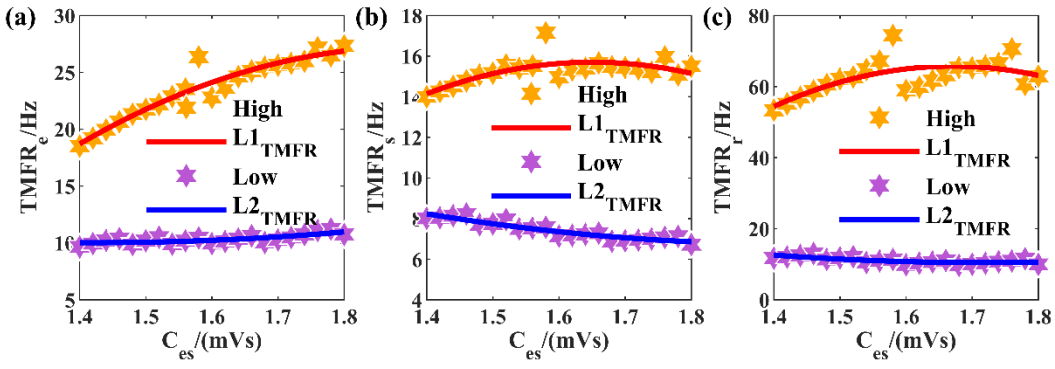

Figure 4. TMFRs of different neurons. (a), (b) and (c), the AMFRs of EPN(a), SRN(b), TRN(c) as a function of C_{es}. The position of orange/purple hex star is determined by the coupling strength of $-C_{sr}$ and C_{es} that trigger absence seizure. L_{1TMFR} and L_{2TMFR} are fitting curves of high and low TMFRs.

3.2. Major parameter selection of constant period m:n on-off SCRS

To test the adaptation of the stimulus to different neurons, single-pulse stimulus with the same intensity but opposite amplitudes were added to each of EPN, SRN and TRN neurons, respectively. The blue line in Figure 5(a) indicates that the amplitude is negative, and the red line indicates that the amplitude is positive. It can be shown from Figure 5(a) that adding negative pulses on neuron EPN or SRN can 100% control the occurrence of epilepsy. Similarly, when positive amplitude single-pulse stimulus was introduced into neuron TRN, SWD could be completely inhibited. Thus, the coordinated stimulus of three neurons was proposed. In other words, positive pulse stimulation was added to EPN and SRN, negative pulse stimulation was added to TRN, and the duration of stimulation to each neuron was controlled through coordinated reset.

Four kinds of m:n on-off SCRS in Figure 5(b) were selected, which were 4:1 on-off SCRS, 3:2 on-off SCRS, 2:3 on-off SCRS, 1:4 on-off SCRS respectively. All four stimuli had the same period $5T_0$, and the effective stimulus duration in a unit period was mT_0. In Figure 5(c), the two indexes of efficacy and energy consumption are combined to investigate the constant period stimulation of different m and n. As can be seen from the purple bar chart (efficacy E), when the effective stimulus duration of SCRS was not lower than $3T_0$, the complete inhibition effect could be achieved. However, once the effective stimulus duration was lower than $3T_0$, the epilepsy control effect showed a trend of continuous decline. Blue broken line graph (energy consumption Q) as the effective stimulus duration decreased, the energy consumption also continuously decreased. Considering the working effect and operating life of electrical stimulator comprehensively, 3:2 on-off SCRS was selected from the four SCRS, which was sufficient to inhibit epilepsy and can extend the life of electrical stimulator relatively. In order to make the 3:2 on-off SCRS play a better role and improve the problem of energy consumption, we would have explored the weighted and closed-loop stimulation in depth in the next chapter.

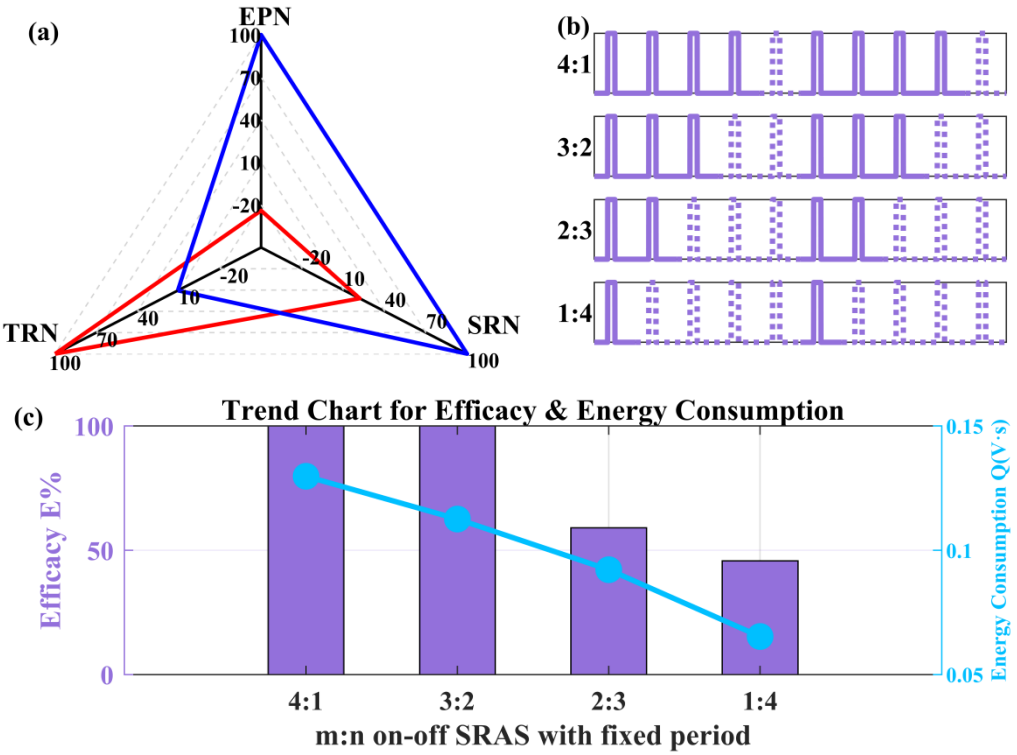

Figure 5. Amplitude and coordinated resetting period of single-pulse stimulation. The three indicators in the radar diagram (a) refer to the efficiency of the stimulation when it is released on the three neurons in the diagram. Select stimulation parameters $|A_0|$ = 200 mA, f_0 = 50 Hz, δ_0 = 3.5 ms. The blue line is a negative amplitude stimulation, and the red line is a positive amplitude stimulation. In diagram (b) of m:n on-off SCRS with constant period, m:n from top to bottom are 4:1, 3:2, 2:3 and 1:4, respectively. In the dual coordinate diagram (c), we combine stimulation efficacy and power consumption to analyze the above four m:n on-off SCRS. The purple bar shows the efficiency of the stimulation, and the blue line shows the energy consumption of four kinds of stimulation.

3.3. Continual improvement of 3:2 on-off SCRS

3.3.1. The weighted calculation of SCRS

Firstly, we plotted the time change diagram of the axon field ϕ_e under different oscillation states of 2I:2O SCT model. In the case of $-C_{sr}$ = 0.8mvs and C_{es} =1.4mvs, the axon field ϕ_e in Figure 6(a_1) presented a simple oscillation state. Similarly, $-C_{sr}$ remains unchanged, C_{es} = 1.8mvs is set, and SWD appears in the axon field ϕ_e in Figure 6(b_1). Figures 6(a_1) and (b_1) correspond to simple oscillations. SWD attractors across EPN, SRN and TRN phase space were shown in Figures 6(a_2) and (b_2). It was noteworthy that the stimulus amplitudes and pulse width of the 3:2 on-off SCRS originally transmitted to neurons EPN, SRN and TRN were identical. As can be seen from Figures 6(a) and (b), the reduction of SWD was related to the change of attractor shape. Therefore, we hypothesized that EPN, SRN and TRN would have different effects with different stimulus intensity.

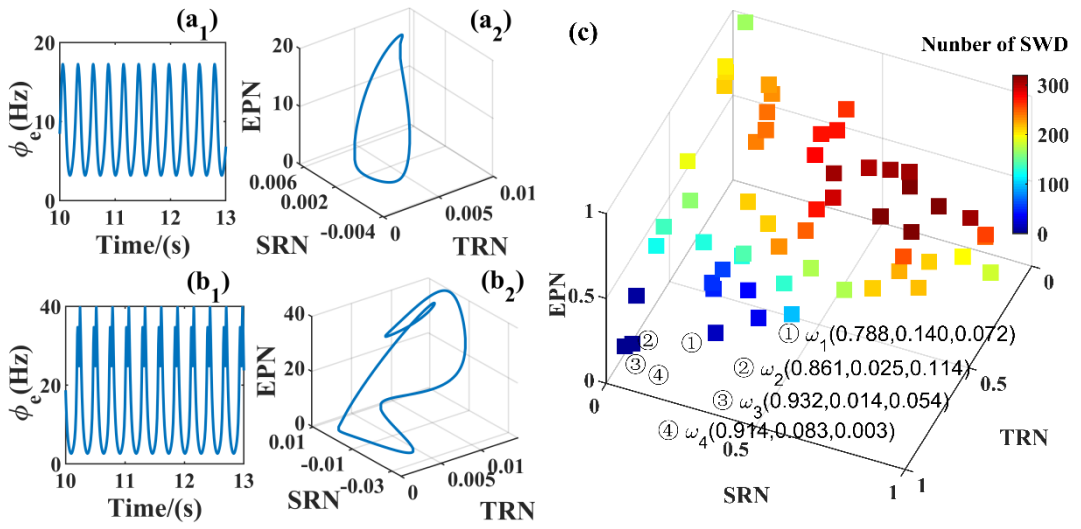

Figure 6. Diagram of oscillating attractors and the weighted 3:2 on-off SCRS. (a_1)–(a_2), in the 2I:2O SCT model, the firing rate ϕ_e waveform and the simple oscillating attractor across three neurons are shown with coupling strength $-C_{sr}$ = 0.8mVs, C_{es} = 1.4 mVs. (b_1)–(b_2), the waveform of axon field ϕ_e and SWD attractor, when $-C_{sr}$ = 0.8mVs, C_{es} = 1.8 mVs. (c), weighted regulation of 3:2 on-off SCRS amplitude and pulse width.

We hoped to obtain 3:2 on-off SCRS with lower energy consumption on the premise of ensuring the therapeutic effect. Here, the stimulation intensity on EPN, SRN and TRN of neurons was weighted, and the weights meet following two conditions: $w_e + w_s + w_r = 1$ and $w_e > 0$, $w_s > 0$, $w_r > 0$. We got the pulse amplitude $\left(A_0^e, A_0^s, A_0^r\right) = A_0\left(w_e, w_s, w_r\right)$, the pulse width $\left(\delta^e, \delta^s, \delta^r\right) = \delta\left(w_e, w_s, w_r\right)$. During the simulation Figure 6(c), 55 random points on the plane $X + Y + Z = 1$ are selected as 55 groups of random weights. The color bar in the figure represented the number of SWD grid points existing after stimulation. It can be seen from Figure 6(c) that SWD grid points may disappear with the increase of pulse weight w_r obtained by TRN. After calculation, the energy consumption was reduced by 2/3 compared with the unweighted stimulation, and the loss of the electric stimulator was greatly reduced. However, the problem was that patients could still receive electrical stimulation during non-seizure periods, which caused unnecessary damage to the patient. In order to improve the effectiveness of stimulation, closed-loop control pulse stimulation would be applied to the model in the following chapters to achieve the regulation of stimulation.

3.3.2. Realization of closed-loop control

In fact, the patient's brain does not need to input electrical pulses all the time, and closed-loop control can effectively solve this problem. The first step was to determine the cortical firing state of epileptic patients. When the recognition result was epileptic state, the system will continuously output pulse stimulation for 60ms. As soon as the patient's brain waves returned to normal, the pulse input was stopped, which greatly reduced the damage to the patient's brain tissue. Referring to previous studies [28], TMFR of cortical neuron EPN could be used as a critical criterion for epileptic seizures in mean-field model simulation. Once the MFR jumped into the range of high/low TMFR, the closed-loop system determined that the network was in a state of disease and activated the stimulus device. According to the above requirements, we designed the following closed-loop control principles:

$$SCRS^{CL}(e) = H(e)\cdot\begin{bmatrix} SCRS_e \\ SCRS_s \\ SCRS_r \end{bmatrix}, \qquad e(t) = MFR_e - TMFR_{y_d}. \tag{26}$$

According to the above principle, we plot a closed-loop control diagram in Figure 7(a). Here, the fitting curve of the trigger average discharge rate in Figure 4(a) is used as the expected value of the closed-loop control. Real-time feedback MFR_e and expected value ($TMFR_{yd}$) were subtracted to calculate the error $e(t)$ at this moment. Here, when designing the controller of the feedback closed-loop system, H is heaviside function, which was used to judge whether the error $e(t)$ was positive.

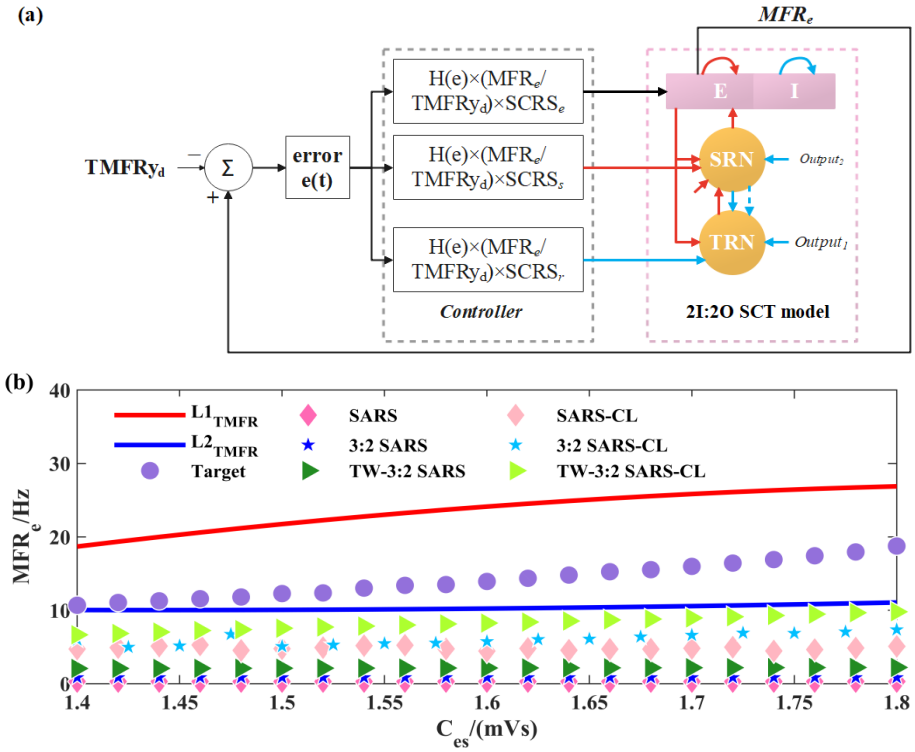

Figure 7. Closed-loop system diagram and effect display. (a), the MFR_e of neuron EPN in 2I:2O SCT model is used as the real-time feedback signal of the system, and the controller allocated the stimulus to the corresponding receptors. (b), first, the red/blue lines fitted by high/low TMFR are used as the critical position of the trigger controller, then the purple circle is set as the therapeutic target, and different markers represent different stimuli. Finally, the changes of MFR_e after stimulation will be shown in the figure.

L_{1TMFR} and L_{2TMFR} were fitting curves of high/low $TMFR_e$. The purple circles (•) in Figure 7(b) corresponding to $-C_{sr}$ = 0.8mVs are all within the range of L_{1TMFR} and L_{2TMFR}. At this point, the brain was seen as a pathogenetic state in the system, MFR under this coupling strength was taken as the target. SCRS, 3:2 on-off SCRS, the weighted 3:2 on-off SCRS in Figure 7(b), i.e. darker markers (♦)(★)(►), suppress cortical MFR to a near-resting state. After filtration by

closed-loop control system, the MFR of the corresponding stimulus increased, that was, the three brighter markers (♦)(★)(►). The results indicated that closed-loop stimulation not only keeps the MFR beyond the critical value, but also reduced the stimulator loss again. Therefore, the closed-loop control successfully realized the real-time monitoring of the patient's status without affecting the therapeutic effect.

The above results showed that whether it was open-loop or closed-loop controlled SARS, 3:2 SARS and TW-3:2 SARS could pull the state of the target back to the normal state. In this case, energy consumption was used as the criterion. Relatively speaking, the comparison of the energy consumption of several electrical stimulations is as follows: SARS>3:2 SARS>TW-3:2 SARS, the energy consumption of closed-loop excitation was also less than that of open-loop excitation. Therefore, the weighted stimulation and closed-loop control methods were adopted to solve the redundancy in energy consumption, and TW-3:2SCRS was finally selected.

4. Conclusions

In this work, a simplified 2I:2O SCT network was constructed based on the existing BGCT model. By adjusting the coupling strength $-C_{sr}$ and C_{es} generated firing patterns in normal and absence epileptic states. The purpose of this study was to obtain optimal control of patients' motor disorders by changing the stimulus pattern.

There are two main contributions to this work. Firstly, it improves the effectiveness of stimulation. In this paper, we selected neurons EPN, SRN and TRN as stimulation targets and considered the effect of positive/negative amplitude pulse stimulation on each of the above neurons, and proposed income constant-period m:n on-off SCR. The results show that the neural network has ideal performance when negative amplitude pulses are added to EPN and SRN, and positive amplitude pulses are added to TRN, and the stimulation is adjusted to 3:2 on-off SCRS. Secondly, a stimulus model based on the weighted method is proposed, which solves the problem of energy consumption in pulse design. Furthermore, a feedback closed-loop control system is designed to compensate for the deficiency of non-real-time open-loop control network without affecting the therapeutic efficacy. The simulation results indicate that both the proposed the weighted method and the feedback closed-loop control strategy can effectively suppress pathological oscillation and have lower energy consumption. Therefore, the results of this investigation can be concluded that the weighted 3:2 on-off SCRS, including feedback closed-loop control strategies, will be a more suitable alternative for regulating absence epileptic states in the future.

Acknowledgments

This work was supported by the National Natural Science Foundation of China (Grant Nos. 12172210 and 11502139). The authors would like to thank the anonymous referees for their efforts and valuable comments.

Conflict of interest

The authors declare that there are no conflicts of interest regarding the publication of this paper.

References

1. A. Vezzani, S. Balosso, T. Ravizza, Neuroinflammatory pathways as treatment targets and biomarkers in epilepsy, *Nat. Rev. Neurol.*, **15** (2019), 459–472. https://doi.org/10.1038/s41582-019-0217-x
2. W. O. Pickrell, M. P. Kerr, SUDEP and mortality in epilepsy: The role of routinely collected healthcare data, registries, and health inequalities, *Epilepsy Behav.*, **103** (2020), 106453. https://doi.org/10.1016/j.yebeh.2019.106453
3. A. Ali, S. Wu, N. P. Issa, S. Rose, V. L. Towle, P. Warnke, et al., Association of sleep with sudden unexpected death in epilepsy, *Epilepsy Behav.*, **76** (2017), 1–6. https://doi.org/10.1016/j.yebeh.2017.08.021
4. E. C. Wirrell, R. Nabbout, I. E. Scheffer, T. Alsaadi, A. Bogacz, J. A. French, et al., Methodology for classification and definition of epilepsy syndromes with list of syndromes: Report of the ILAE Task Force on Nosology and Definitions, *Epilepsia*, **63** (2022), 1333–1348. https://doi.org/10.1111/epi.17237
5. M. Bosak, A. Słowik, R. Kacorzyk, W. Turaj, Implementation of the new ILAE classification of epilepsies into clinical practice—A cohort study, *Epilepsy Behav.*, **96** (2019), 28–32. https://doi.org/10.1016/j.yebeh.2019.03.045
6. C. M. Korff, I. E. Scheffer, Epilepsy classification: a cycle of evolution and revolution, *Curr. Opin. Neurol.*, **26** (2013), 163–167. https://doi.org/10.1097/WCO.0b013e32835ee58e
7. S. A. Demin, O. Y. Panischev, S. F. Timashev, R. R. Latypov, Analysis of Interictal EEG Signal Correlations for Diagnostics of Epilepsy, *Bull. Russ. Acad. Sci. Phys.*, **84** (2020), 1349–1353. https://doi.org/10.3103/S1062873820110088
8. R. Sharma, R. B. Pachori, Classification of epileptic seizures in EEG signals based on phase space representation of intrinsic mode functions, *Expert Syst. Appl.*, **42** (2015), 1106–1117. https://doi.org/10.1016/j.eswa.2014.08.030
9. H. Soh, R. Pant, J. J. LoTurco, A. V. Tzingounis, Conditional deletions of epilepsy-associated KCNQ2 and KCNQ3 channels from cerebral cortex cause differential effects on neuronal excitability, *J. Neurosci.*, **34** (2014), 5311–5321. https://doi.org/10.1523/JNEUROSCI.3919-13.2014
10. P. A. Winkler, C. Vollmar, K. G. Krishnan, T. Pfluger, H. Brückmann, S. Noachtar, Usefulness of 3-D reconstructed images of the human cerebral cortex for localization of subdural electrodes in epilepsy surgery, *Epilepsy Res.*, **41** (2000), 169–178. https://doi.org/10.1016/S0920-1211(00)00137-6
11. J. T. Paz, T. J. Davidson, E. S. Frechette, B. Delord, I. Parada, K. Peng, et al., Closed-loop optogenetic control of thalamus as a tool for interrupting seizures after cortical injury, *Nat. Neurosci.*, **16** (2013), 64–70. https://doi.org/10.1038/nn.3269
12. N. Li, J. E. Downey, A. Bar-Shir, A. A. Gilad, P. Walczak, H. Kim, et al., Optogenetic-guided cortical plasticity after nerve injury, *Proc. Natl. Acad. Sci. USA*, **108** (2011), 8838–8843. https://doi.org/10.1073/pnas.1100815108
13. L. van Veen, K. R. Green, Periodic solutions to a mean-field model for electrocortical activity, *Eur. Phys. J. Spec. Top.*, **223** (2014), 2979–2988. https://doi.org/10.1140/epjst/e2014-02311-y
14. P. N. Taylor, Y. Wang, M. Goodfellow, J. Dauwels, F. Moeller, U. Stephani, et al., A computational study of stimulus driven epileptic seizure abatement, *PLoS One*, **9** (2014), e114316. https://doi.org/10.1371/journal.pone.0114316

15. M. Chen, D. Guo, T. Wang, W. Jing, Y Xia, P. Xu, et al., Bidirectional control of absence seizures by the basal ganglia: A computational evidence, *PLoS Comput. Biol.*, **10** (2014), e1003495. https://doi.org/10.1371/journal.pcbi.1003495
16. I. S. Cooper, A. R. Upton, I. Amin, Chronic cerebellar stimulation (CCS) and deep brain stimulation (DBS) in involuntary movement disorders, *Appl. Neurophysiol.*, **45** (1982), 209–217. https://doi.org/10.1159/000101601
17. S. F. Lempka, M. D. Johnson, S. Miocinovic, J. L. Vitek, C. C. McIntyre, Current-controlled deep brain stimulation reduces in vivo voltage fluctuations observed during voltage-controlled stimulation, *Clin. Neurophysiol.*, **121** (2010), 2128–2133. https://doi.org/10.1016/j.clinph.2010.04.026
18. R. G. Cury, V. Fraix, A. Castrioto, M. A. P. Fernández, P. Krack, C. S. habardes, et al., Thalamic deep brain stimulation for tremor in Parkinson disease, essential tremor, and dystonia, *Neurology*, **89** (2017), 1416–1423. https://doi.org/10.1212/WNL.0000000000004295
19. V. A. Coenen, N. Allert, B. Mädler, A role of diffusion tensor imaging fiber tracking in deep brain stimulation surgery: DBS of the dentato-rubro-thalamic tract (drt) for the treatment of therapy-refractory tremor, *Acta. Neurochir.*, **153** (2011), 1579–1585. https://doi.org/10.1007/s00701-011-1036-z
20. R. Arya, H. M. Greiner, A. Lewis, F. T. Mangano, C. Gonsalves, K. D. Holland, et al., Vagus nerve stimulation for medically refractory absence epilepsy, *Seizure*, **22** (2013), 267–270. https://doi.org/10.1016/j.seizure.2013.01.008
21. Z. Ye, L. McQuillan, A. Poduri, T. E. Green, N. Matsumoto, H. C. Mefford, et al., Somatic mutation: the hidden genetics of brain malformations and focal epilepsies, *Epilepsy Res.*, **155** (2019), 106161. https://doi.org/10.1016/j.eplepsyres.2019.106161
22. E. A. Van Vliet, E. Aronica, A. Vezzani, T. Ravizza, Neuroinflammatory pathways as treatment targets and biomarker candidates in epilepsy: emerging evidence from preclinical and clinical studies, *Neuropath. Appl. Neuro.*, **44** (2018), 91–111. https://doi.org/10.1111/nan.12444
23. T. Lundgren, J. Dahl, N. Yardi, L. Melin, Acceptance and commitment therapy and yoga for drug-refractory epilepsy: A randomized controlled trial, *Epilepsy Behav.*, **13** (2008), 102–108. https://doi.org/10.1016/j.yebeh.2008.02.009
24. C. Joint, D. Nandi, S. Parkin, R. Gregory, T. Aziz, Hardware-related problems of deep brain stimulation, *Movement Disord.*, **17** (2002), S175–S180. https://doi.org/10.1002/mds.10161
25. Z. Peng-Chen, T. Morishita, D. Vaillancourt, C. Favilla, K. D. Foote, M. S. Okun, et al., Unilateral thalamic deep brain stimulation in essential tremor demonstrates long-term ipsilateral effects, *Parkinsonism Relat. Disord.*, **19** (2013), 1113–1117. https://doi.org/10.1016/j.parkreldis.2013.08.001
26. M. K. Hosain, A. Kouzani, S. Tye, Closed loop deep brain stimulation: an evolving technology, *Australas. Phys. Eng. Sci. Med.*, **37** (2014), 619–634. https://doi.org/10.1007/s13246-014-0297-2
27. J. Volkmann, E. Moro, R. Pahwa, Basic algorithms for the programming of deep brain stimulation in Parkinson's disease, *Movement Disord.*, **21** (2006), S284–S289. https://doi.org/10.1002/mds.20961
28. D. Fan, Q. Wang, Closed-loop control of absence seizures inspired by feedback modulation of basal ganglia to the corticothalamic circuit, *IEEE Trans. Neur. Sys. Reh.*, **28** (2020), 581–590. https://doi.org/10.1109/TNSRE.2020.2969426

29. C. Liu, J. Wang, B. Deng, X. Wei, H. Yu, H. Li, et al., Closed-loop control of tremor-predominant parkinsonian state based on parameter estimation, *IEEE Trans. Neur. Sys. Reh.*, **24** (2016), 1109–1121. https://doi.org/10.1109/TNSRE.2016.2535358
30. B. Rosin, M. Slovik, R. Mitelman, M. Rivlin-Etzion, S. N. Haber, Z. Israel, et al., Closed-loop deep brain stimulation is superior in ameliorating parkinsonism, *Neuron*, **72** (2011), 370–384. https://doi.org/10.1016/j.neuron.2011.08.023
31. B. Hu, Q. Wang, Controlling absence seizures by deep brain stimulus applied on substantia nigra pars reticulata and cortex, *Chaos Soliton. Fract.*, **80** (2015), 13–23. https://doi.org/10.1016/j.chaos.2015.02.014
32. C. Liu, J. Wang, H. Li, C. Fietkiewicz, K. A. Loparo, Modeling and analysis of beta oscillations in the basal ganglia, *IEEE Trans. Neur. Net. Lear. Sys.*, **29** (2017), 1864–1875. https://doi.org/10.1109/TNNLS.2017.2688426
33. P. A. Robinson, P. N. Loxley, S. C. O'connor, C. J. Rennie, Modal analysis of corticothalamic dynamics, electroencephalographic spectra, and evoked potentials, *Phys. Rev. E*, **63** (2001), 041909. https://doi.org/10.1103/PhysRevE.63.041909
34. V. K. Jirsa, H. Haken, Field theory of electromagnetic brain activity, *Phys. Rev. Lett.*, **77** (1996), 960. https://doi.org/10.1103/PhysRevLett.77.960
35. D. L. Rowe, P. A. Robinson, C. J. Rennie, Estimation of neurophysiological parameters from the waking EEG using a biophysical model of brain dynamics, *J. Theor. Biol.*, **231** (2004), 413–433. https://doi.org/10.1016/j.jtbi.2004.07.004
36. S. Coombes, Large-scale neural dynamics: simple and complex, *NeuroImage*, **52** (2010), 731–739. https://doi.org/10.1016/j.neuroimage.2010.01.045
37. D. Terman, J. E. Rubin, A. C. Yew, C. J. Wilson, Activity patterns in a model for the subthalamopallidal network of the basal ganglia, *J. Neurosci.*, **22** (2002), 2963–2976. https://doi.org/10.1523/JNEUROSCI.22-07-02963.2002
38. M. E. Anderson, N. Postupna, M. Ruffo, Effects of high-frequency stimulation in the internal globus pallidus on the activity of thalamic neurons in the awake monkey, *J. Neurophysi.*, **89** (2003), 1150–1160. https://doi.org/10.1152/jn.00475.2002
39. A. Benazzouz, D. M. Gao, Z. G. Ni, B. Piallat, R. Bouali-Benazzouz, A. L. Benabid, Effect of high-frequency stimulation of the subthalamic nucleus on the neuronal activities of the substantia nigra pars reticulata and ventrolateral nucleus of the thalamus in the rat, *Neuroscience*, **99** (2000), 289–295. https://doi.org/10.1016/S0306-4522(00)00199-8
40. Z. Wang, Q. Wang, Stimulation strategies for absence seizures: targeted therapy of the focus in coupled thalamocortical model, *Nonlinear Dyn.*, **96** (2019), 1649–1663. https://doi.org/10.1007/s11071-019-04876-z
41. D. Fan, Y. Zheng, Z. Yang, Q. Wang, Improving control effects of absence seizures using single-pulse alternately resetting stimulation (SARS) of corticothalamic circuit, *Appl. Math. Mech.*, **41** (2020), 1287–1302. https://doi.org/10.1007/s10483-020-2644-8
42. M. Chen, D. Guo, M. Li, T. Ma, S. Wu, J. Ma, et al., Critical roles of the direct GABAergic pallido-cortical pathway in controlling absence seizures, *PLoS Comput. Biol.*, **11** (2015), e1004539. https://doi.org/10.1371/journal.pcbi.1004539

AIMS Press